Substituent Effects on Singlet Exciton Fission in Polycrystalline Thin Films of Cyano-Substituted Diaryltetracenes

Eric A. Margulies,[†] Nicolas Kerisit,[‡] Przemyslaw Gawel,[‡] Catherine M. Mauck,[†] Lin Ma,[†] Claire E. Miller,[†] Ryan M. Young,[†] Nils Trapp,[‡] Yi-Lin Wu,*,[†] Francois Diederich,*,[‡] and Michael R. Wasielewski*,[†]

[†]Department of Chemistry, Argonne-Northwestern Solar Energy Research (ANSER) Center, and Institute for Sustainability and Energy at Northwestern (ISEN), Northwestern University, Evanston, Illinois 60208-3113, United States

[‡]Laboratorium fürOrganische Chemie, ETH Zürich, CH-8093 Zürich, Switzerland

* Supporting Information

ABSTRACT: Cyano-substituted tetracenes (5,11-dicyano-6,12-diphenylte-tracene, Tet) undergo exoergic singlet fission (SF), a spin-allowed photophysical process that generates a pair of triplet excitons from one singlet exciton. To elucidate substituent effects on SF, we have measured the SF dynamics and triplet yields of thin films, formed by Tet bearing hydrogen (H), methyl (Me), fluoro (F), and trimethylsilyl (TMS) substituents on the p-phenyl positions and on the 3 and 9 positions of the tetracene core, by time-resolved spectroscopy in the vis-NIR and IR regions. The H-, Me-, and F-Tet display strong intramolecular electronic coupling (π−π distances <4 Å), and SF gives high triplet exciton yields up to 200% (quantitative). In addition, a charge-transfer state mediates SF in F-Tet films, while H-Tet and Me-Tet show no evidence for such a state. Correlations between the SF yields and the crystal structure show that chromophore slippage along both their short and long axes allows efficient SF and that a large degree of π contact between the chromophores is not necessary for rapid and efficient SF in the solid state. As expected, the large interchromophore distance in TMS-Tet (>4 Å) reduces its SF triplet yield to about 60%.
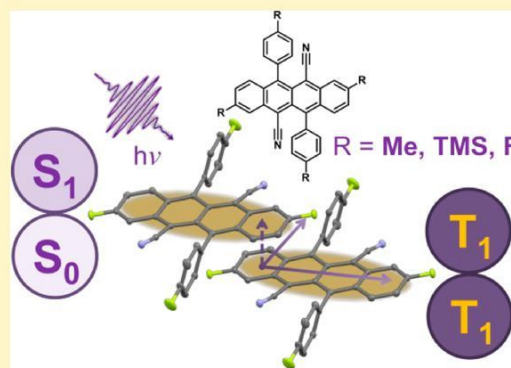
INTRODUCTION

Singlet fission (SF), a process that converts one singlet exciton (S_1) to a pair of triplet excitons (T_1) on coupled chromophores, offers a potential route to increase the efficiency of solar cells. Analogous to multiple exciton generation (MEG) in inorganic nanocrystals, the carrier multiplication afforded by SF can be used in conjunction with a conventional absorber leading to a maximum theoretical device efficiency of 45%,[1,2] much higher than the 33% Shockley-Queisser limit.[3] The SF mechanism couples the $^1(S_1S_0)$ state to the $^1(T_1T_1)$ triplet-pair state that has overall singlet character, thus allowing for spin conservation, which may result in ultrafast and highly efficient SF when $E(S_1) \geq 2E(T_1)$.

SF necessitates the transfer of two electrons,[4] which may be achieved by one of two mechanisms: either directly through a two-electron process,[1,5−7] or by two one-electron charge transfer (CT) processes. The exact mechanism remains unclear, but both mechanisms may be at play to varying degrees and the states involved may be of mixed nature.[8−11] For SF to proceed efficiently by the sequential one-electron CT mechanism, the CT state energy must lie between that of the $^1(S_1S_0)$ and $^1(T_1T_1)$ states; however, this is rarely the case, as CT energies are generally well above the S_1 energy. Alternatively, the electronic coupling matrix elements for a one-electron process

are much larger than that of a two-electron process, often by up to 2 orders of magnitude,[11] and it is unlikely that the coupling for the direct two-electron process is sufficient to produce the ultrafast SF rates observed.[4] Recently, SF has been proposed to occur by a superexchange mechanism involving a virtual CT state,[4] much like many electron transfer processes in donor-bridge-acceptor molecules.[12−14] Coupling the $^1(S_1S_0)$ and CT states allows for an overall electronic coupling matrix element that is a function of both the one- and two-electron matrix elements, resulting in a coupling value large enough for SF to occur on an ultrafast time scale.

Originally discovered in acenes through the observation of unexpected delayed fluorescence phenomena,[15−17] SF has subsequently been observed in a much broader range of chromophores including polyenes,[18−20] rylenes,[21−23] semiconducting polymers and oligomers,[24,25] and other aromatic chromophores.[26−28] Due to their early discovery and largely suitable energetics, the acene family continues to serve as a benchmark for SF investigations.[8,9,29−39] For example, pentacene satisfies the energetic requirements for SF leading to exoergic SF, whereas tetracene has slightly endoergic SF,

partially due to strong intermolecular coupling in solids that lowers the S_1 energy, leading to a much slower SF rate than pentacene. Substitution on the 5 and 12 positions of tetracene with phenyl groups was found to reduce such coupling, evident by the similar solution and solid phase absorption spectra, which allows for rapid singlet fission even in the largely amorphous aggregates.[36] Additionally, we recently demonstra-ted that the tetracene packing and energetics can be altered further by synthetic modifications, resulting in efficient SF in 5,11-dicyano-6,12-diphenyltetracene.[40] An increase in diradical character induced by the cyano and phenyl substituents leads to a stabilized triplet state and rapid SF.
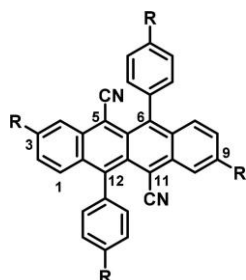
Tet, R = H, Me, TMS, F

In this report, we examine how methyl (Me-Tet), trimethylsilyl (TMS-Tet), and fluoro (F-Tet) substitution of the tetracene core at positions 3 and 9, as well as at the p-phenyl positions of 5,11-dicyano-6,12-diphenyltetracene, affects SF in thin film samples of these molecules. In this series, H-, Me-, and TMS-Tet have similar electronic properties and thus allow for structural comparisons. The relationship of molecular structure measured by single crystal and thin-film grazing incidence X-ray diffraction (GIXRD) to the SF rate and efficiency measured by transient optical spectroscopy reveals the importance of intermolecular electronic coupling and CT character in the tetracene SF process.

EXPERIMENTAL SECTION

Sample Preparation. The synthesis and crystal structures of the functionalized cyano-substituted diaryltetracenes H-Tet and Me-Tet were described previously,[41] while those of TMS-Tet, and F-Tet are reported in the Supporting Information (SI), Section S1. All derivatives were further purified by gradient sublimation ($250-320$ °C, 10^{-6} Torr) prior to thin-film preparation. Thin film samples were prepared by thermal evaporation onto glass (ArrayIt SuperClean 2) or polished sapphire substrates (25.4 mm diameter × 1 mm thickness, Ted Pella, Inc. Redding, CA) using an Angstrom Engineering Covap II system. Thin film samples were solvent-vapor annealed by exposure to CH_2Cl_2 vapor for up to 2 h to increase crystallinity.

Film Characterization. Film thicknesses were determined using a Veeco Dektak 150 surface profilometer equipped with a 25 μm diameter stylus. GIXRD measurements were performed using a Rigaku SmartLab XRD system with a 0.2° incident angle. The resulting diffractograms were manually background subtracted using PDXL software.

Steady-State Optical Characterization. Solution UV/vis absorption spectra were acquired using a Shimadzu 1800 spectrophotometer. Scatter-corrected absorption spectra of the thin film samples were acquired using a PerkinElmer LAMBDA 1050 UV/vis/NIR spectrophotometer equipped with an integrating sphere (150 mm). The scatter-free absorbance (A) was calculated using the transmittance (T) and reflectance

(R) of the thin film samples: $A = -\log(T + R)$. FTIR spectra were measured on a Shimadzu IRAffinity-1 spectrophotometer.

Transient Optical Characterization. Femtosecond- and nanosecond transient absorption (fsTA and nsTA, respectively) measurements were performed using previously described instrumentation.[40,42] For the thin-film samples, the low-fluence (100 kHz, 20 nJ, $\sim10^{17}$ cm^{-3} excitation density) measurements provided transient spectra and kinetics in the $520-800$ nm range free from singlet−singlet annihilation, while high fluence (1 kHz, 1 μJ, $\sim10^{19}$ cm^{-3} excitation density) experiments were also conducted to cover the wider $450-1600$ nm range. Femtosecond transient IR (fsIR) spectra were collected with 550 or 570 nm (2 μJ/pulse) excitation using an instrument described elsewhere.[43] Films for fsIR were vapor-deposited on CaF_2 slides (2 mm thickness, Red Optronics) and stored in the dark under an inert atmosphere prior to measurement. All fsIR spectra were collected under N_2 by enclosing the samples in a high-temperature solid cell with NaCl windows (Harrick Scientific). Global analysis of each transient data set was performed according to methods described in the SI.

RESULTS

Dimer Pair Geometry. Since SF is assumed to primarily involve nearest-neighbor chromophore pair interactions,[11] the relative geometry of this interaction in the crystal structure is analyzed to identify important dimer interactions. We find that all derivatives pack in a π-stacked motif unlike the herringbone structure observed in tetracene.[44] This difference, attributed to the disruption of favorable CH−π interactions by functionaliza-tion of the tetracene edge positions,[45] results in a higher degree of π-overlap between neighboring chromophores. Similar π-stacking geometry was also found in highly efficient SF 5,12-diphenyltetracene, where neighboring tetracenes slip slightly along the molecular long axis ($\sim3-4$ benzene-ring overlap) with π−π spacing ~3.8 Å.[36] Functionalization of the phenyl groups and the 3 and 9 positions of the tetracene core results in alteration of the crystal structures that affects interactions within the dimers. These dimer pairs and their relative geometries are depicted in Figure 1 and summarized in Table 1.

Notably, the unfunctionalized H-Tet derivative has a crystal structure with partially intercalated π-stacks. This results in two different π-stacking interactions labeled α and β. Within one stack (the α interaction), the π-contact is relatively poor with a
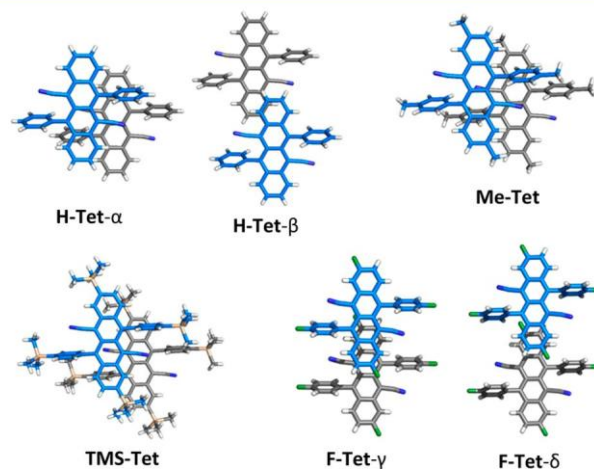

Figure 1. Top-down view of the dimer pair geometry in the crystal structure of H-, Me-, TMS-, and F-Tet.

Table 1. Summary of the Molecular Offsets Exhibited in Pairs of Molecules in the H-, Me-, TMS-, and F-Tet Crystal Structures

		long axis (Å)	short axis (Å)	π−π (Å)
H-Tet[a]	α	1.87	3.63	4.06
	β	7.88	2.16	3.31
Me-Tet		1.43	3.55	3.94
TMS-Tet		2.34	3.50	4.17
F-Tet[a]	γ	6.06	0.71	3.46
	δ	8.21	0.17	3.47

[a]See Figure 1 for the α, β and γ, δ geometries.

4.06 Å spacing between adjacent chromophores. The second, β, interaction is highly slipped, with a 7.88 Å offset in the tetracene long axis, which results in less than one benzene ring of each tetracene experiencing π-overlap. This interaction, however, has a much closer π−π distance of 3.31 Å. The Me-Tet derivative has an interaction resembling the α interaction of H-Tet, but with a slightly smaller slip distance in the long and short axes and a slightly closer π−π distance of 3.94 Å. The bulky TMS substituent in TMS-Tet greatly disrupts the π-stacking and results in an interaction also similar to the H-Tet α interaction, but with a large π−π distance of 4.17 Å. The smaller atomic radius of the fluorine atom in F-Tet results in short π−π contacts of ∼3.46 Å for two similar long-axis slipped dimer pairs.

Excited-State Dynamics of Monomeric Tetracenes. To evaluate the excited state dynamics of the monomeric Tet derivatives, fsTA spectroscopy was performed on the three compounds in CH_2Cl_2 solution (Figure 2). For reference, the absorption spectra of Me-, TMS-, and F-Tet solutions are shown in Figure 4, where they are compared with those of the thin films. The steady-state spectra are nearly identical in
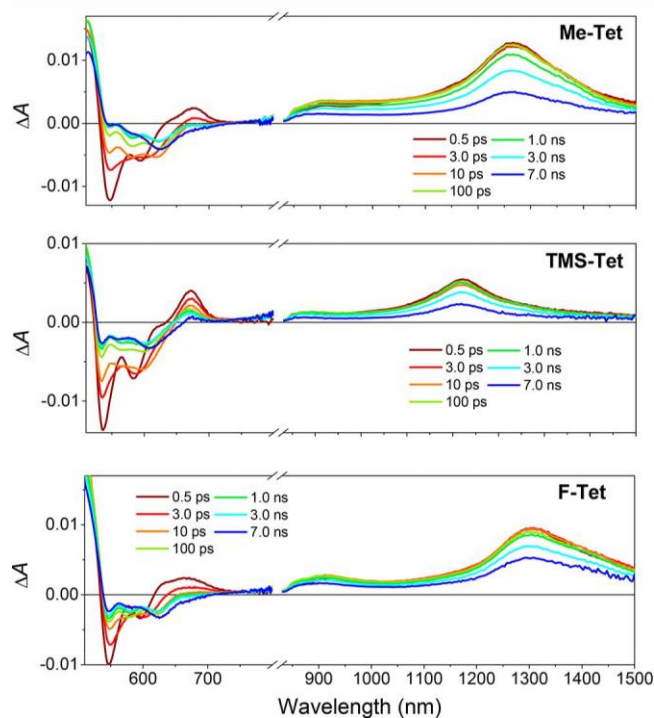

Figure 2. Solution fsTA spectra of Me-, TMS-, and F-Tet in CH_2Cl_2 excited at 500 nm (0.6 μJ/pulse).

vibronic progression and relative band intensities, with a slight substituent shift (<50 meV) in the S_1 energy across the series. These chromophores all have a clearly resolved and strong singlet excited state absorption (ESA) feature in the NIR region (∼1250 nm). This feature is unique to the S_1 state, and absent in the T_1 state, which will be discussed later. The excited-state decay kinetics indicate that the substituents do not greatly alter the nature or lifetime of the excited state relative to H-Tet. Following excitation near 500 nm, there is an initial, rapid ∼2 ps decay across the spectrum, followed by a slower, tens of ps relaxation, and then the terminal ∼10 ns decay of the entire spectrum. At early times, the ground state bleach (GSB) near 545 nm appears to diminish, however, the stimulated emission (SE) in the 600 nm region remains intense in each case. The shape of the ESA feature in the NIR region also remains unchanged. Global analysis using a sequential decay model (see SI, Section S5) shows that the spectral changes are limited to the region near the GSB signal. We attribute the ∼2 ps process to intramolecular vibrational relaxation (IVR) along the S_1 surface owing to excitation above the optical bandgap. As in our previous study, the slower ∼10s of ps process is assigned to a rotation of the phenyl substituents to adopt a more stable geometry in the singlet excited state,[40] which alters the excited state oscillator strength. The substitution also has little effect on the excited state lifetime with all derivatives exhibiting a long S_1 lifetime of τ ∼ 10 ns.

Film Structural Analysis. The crystallinity of the film samples was evaluated using GIXRD (Figure 3). We find that vapor deposition of Me-Tet on room-temperature substrates results in a relatively crystalline film that changes only slightly upon solvent-vapor annealing. The peak shape, especially at small angles, is likely influenced by the slight preferred orientation of the [1 0 2̄] direction and small crystallite-caused line broadening. Owing to a much poorer association of chromophores in the crystal structure, TMS-Tet films begin highly amorphous with very little diffraction. Solvent-vapor annealing produces large changes in the diffraction pattern, yielding a strongly diffracting film with clear peaks due to the (100) and (101) planes, which is consistent with a tilted long axis end-on alignment of the tetracene relative to the plane of the substrate. Solvent-vapor annealing of F-Tet produces a highly oriented film. The unannealed film exhibits a strong diffraction peak from the (001) plane as well as the (0 1 1̄) and (1 1̄ 0)/(101) planes in addition to some amorphous scatter around 25°. Annealing greatly reduces the intensity of the (1̄) diffraction peak and enhances the (0 1 1̄) and (1 1̄ 0)/ (101) peaks, which indicates a shift to a more oriented film with more long axis end-on packing on the substrate.

Thin-Film Optical Characterization. Scatter-corrected ground state absorption spectra of the three thin film samples are shown in Figure 4. Films of Me-Tet and F-Tet show clear signs of aggregation with a very different absorption spectrum relative to their solution spectra. Both compounds exhibit a strong enhancement of the blue region of their absorption spectra as well as a red shift of their absorption maxima in the solid state. The Me-Tet film exhibits a larger enhancement of the 0−1 and 0−2 bands than the enhancement observed in H-Tet, relative to the 0−0 peak.[40] This difference is likely due in part to the nature of the interaction between neighboring chromophores in the two crystal structures. With the transition dipole oriented along the tetracene short axis,[46] it is expected that shifts in this direction would most significantly affect the dipolar coupling and thus the absorption spectrum.[47]
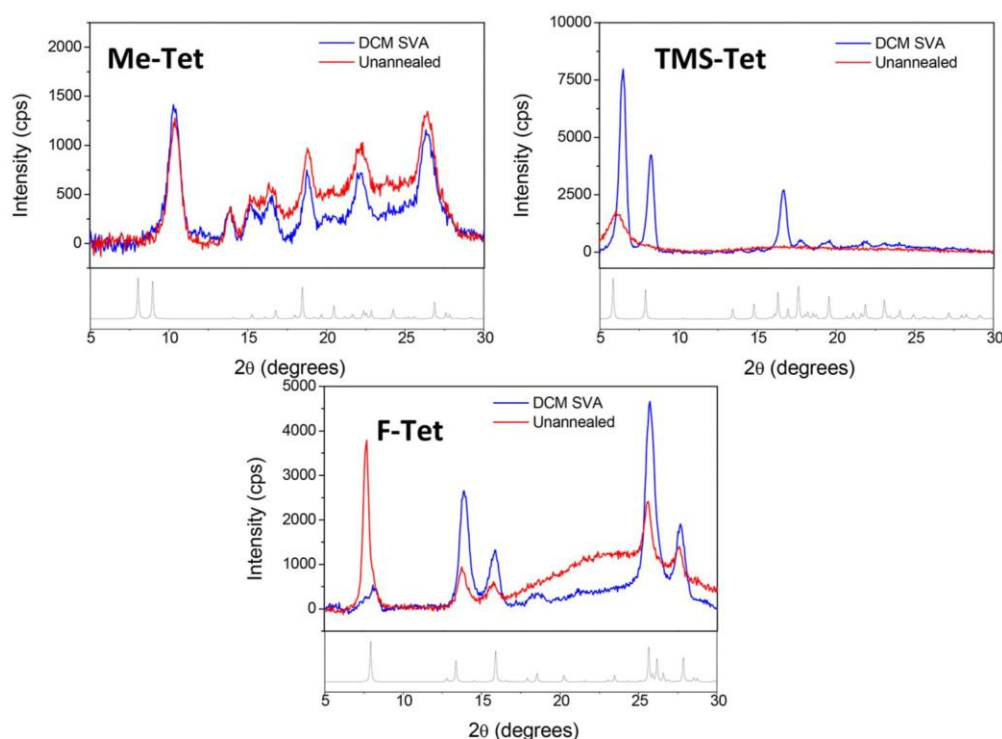
Figure 3. Grazing incidence diffractograms of unannealed (red) and CH_2Cl_2 solvent-vapor annealed (DCM SVA, blue) films of Me-, TMS-, and F-Tet. Powder patterns simulated from the respective crystal structures are shown in black.
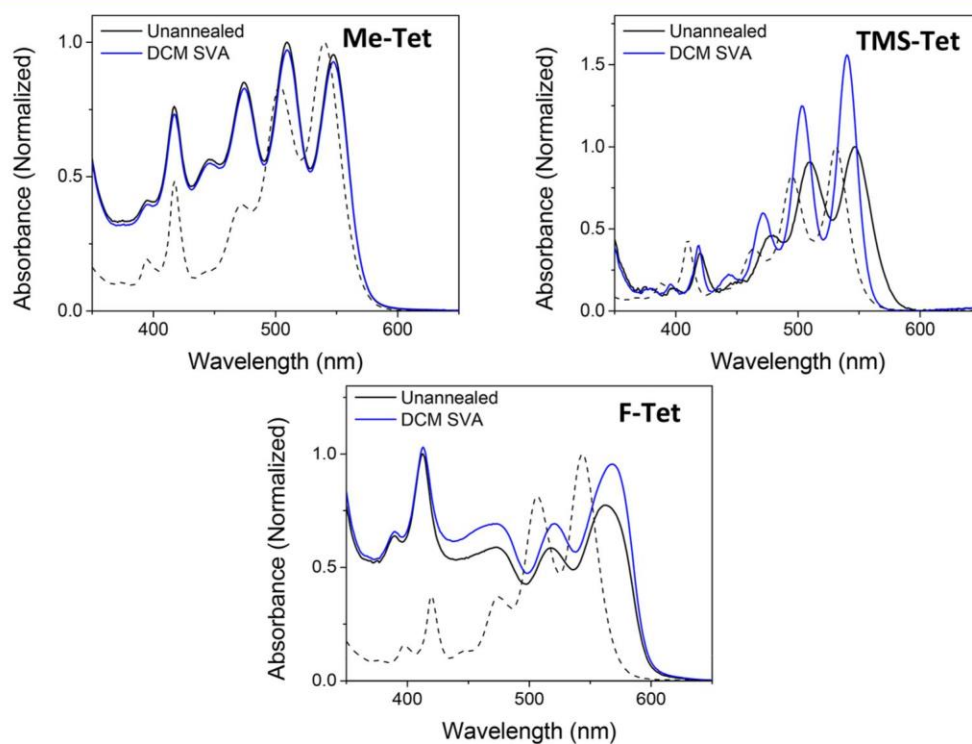

Figure 4. Normalized solution (dashed) and film (black) absorption spectra of Me-, TMS-, and F-Tet. The absorption spectra of the solvent vapor annealed films (blue) are normalized using the unannealed spectra.

Comparing the dimer pair of Me-Tet to the α dimer pair of H-Tet, the short axis slip distance is smaller in Me-Tet and the π−π distance is closer giving rise to these differences. Annealing the F-Tet film significantly increases the intensity of the overall absorption spectrum, which is consistent with the increased long axis end-on alignment observed in the annealed film by GIXRD. End-on orientation increases the alignment of the short axis and, thus, the transition dipole, with the electric field of the light oriented perpendicular to the substrate. This results in increased light absorption by the oriented film.

Owing to much weaker intermolecular coupling, the absorption spectra of the TMS-Tet films more closely resemble
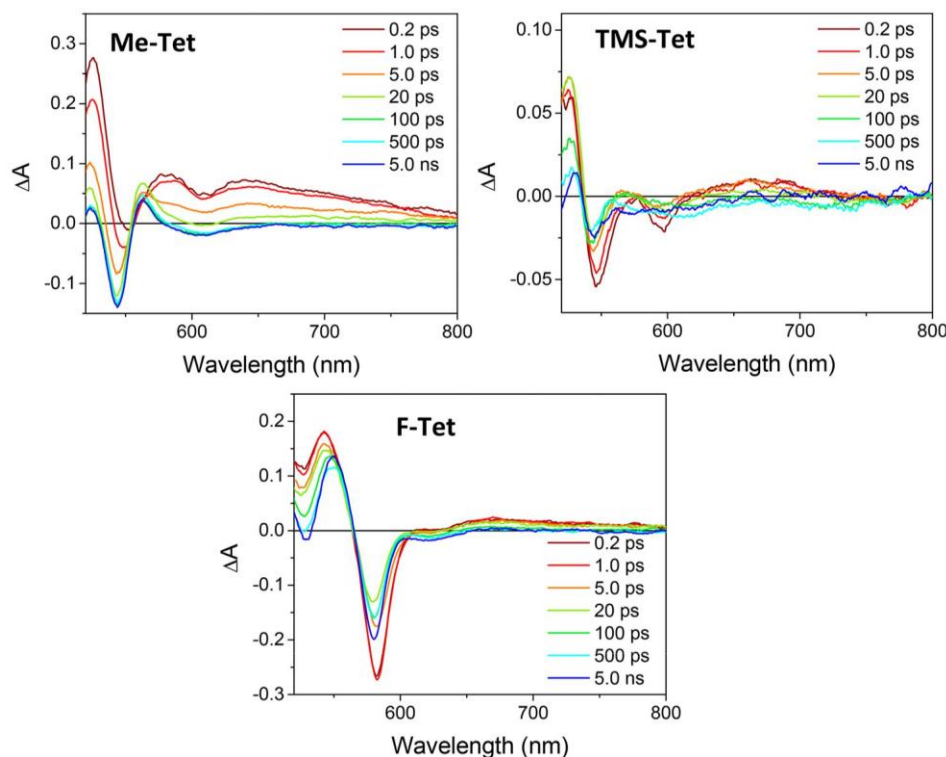
Figure 5. Low fluence fsTA spectra of annealed Me-, TMS-, and F-Tet thin films following 510 nm excitation ($\sim10^{17}$ cm^{-3}).

the solution spectrum. The unannealed film exhibits an absorption spectrum nearly identical to that of the compound in solution except for a 15 nm red shift and a general broadening characteristic of gas-to-crystal effects in the solid state. However, there are no clear signs of strong coupling between the molecular transition dipoles, which depends on $1/r^3$, in concert with the longer distance between the molecules enforced by the steric bulk of the TMS group. Interestingly, annealing reduces this red shift and sharpens the absorption bands. This change implies that packing of the TMS-Tet compound is closer, on average, in the amorphous arrangement than the 4.17 Å distance exhibited in the crystalline morphology. Annealing also greatly enhances the absorption intensity by roughly a factor of 1.5. This is in agreement with the GIXRD measurements, which indicate a tilted long axis end-on arrangement of the chromophore on the substrate in the annealed sample.

Thin Film Transient Absorption Measurements. Given the higher crystallinity of the CH$_2$Cl$_2$-vapor annealed thin films compared to the as-deposited ones, we focus the time-resolved SF studies on the annealed films. Figure 5 shows the low-fluence, singlet−singlet annihilation-free fsTA spectra after photoexcitation of the annealed Me-Tet film (λ_{exc} = 510 nm), which are similar to those of the parent chromophore, H-Tet.[40] High fluence transient spectra are shown in Figures 6 and S9. At short time delays after the pump pulse, we find a characteristic singlet spectrum with broad ESA having a maximum at 525 nm and a broad feature out to 800 nm. The ESA signal overlaps the negative SE feature resulting in a minimum at 610 nm, most of which disappears in a few picoseconds. The GSB also overlaps the ESA and has a clearly resolved minimum at $\sim$550 nm. These S$_1$ features decay over time to produce the characteristic triplet spectrum with maxima adjacent to the GSB in the visible and no NIR absorption. The small amount of residual stimulated emission observed at 610
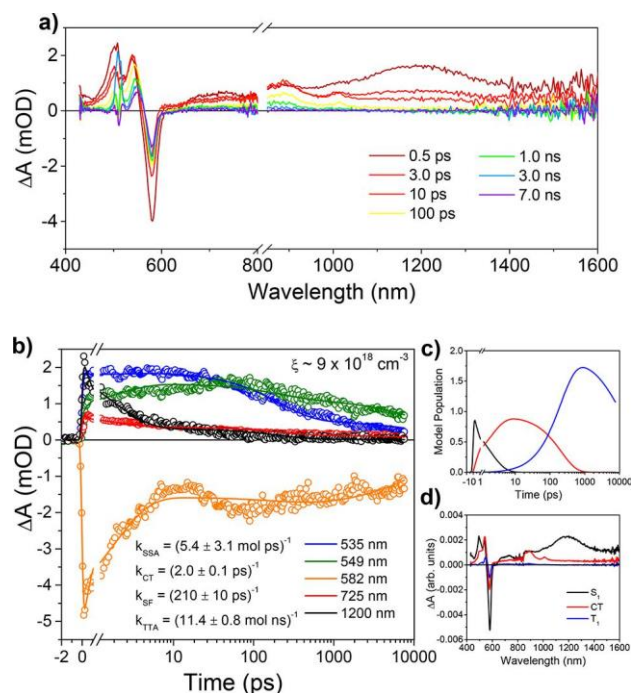
Figure 6. (a) Visible and near-infrared fsTA spectra of solvent-vapor annealed F-Tet film following 510 nm excitation ($\sim10^{19}$ cm^{-3}). (b) Global fits to eq S3. (c) Solutions to the kinetic model. (d) Reconstructed species-associated spectra. The analysis indicates that the 2 ps loss of the singlet state ($\sim$1200 nm) is concomitant with the growth of the NIR feature (895 and 1010 nm) and that the $\sim$200 ps decay of this species is associated with the growth of a triplet absorption feature at 560 nm.

nm at longer times ($\sim$5 ns) may be due to triplet−triplet fusion occurring at defect sites within the film, where the rapidly

Table 2. Kinetic Parameters for Thin Film Samples Obtained from Global Analysis

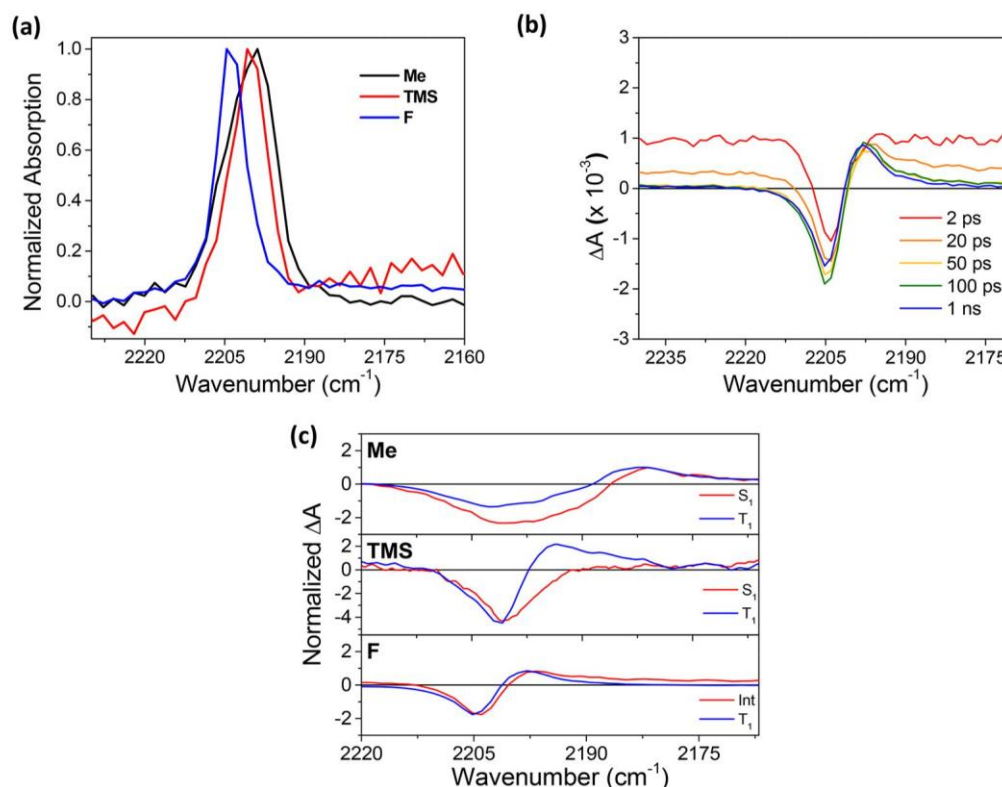| ξ (cm^{-3})	τ_{relax} (ps)		τ_{CT} (ps)		τ_{SF} (ps)		k_{TTA} (mol^{-1} s^{-1})	
	$\sim 10^{17}$	$\sim 10^{19}$	$\sim 10^{17}$	$\sim 10^{19}$	$\sim 10^{17}$	$\sim 10^{19}$	$\sim 10^{17}$	$\sim 10^{19}$
Me-Tet	1.3 ± 0.3	2.2 ± 0.1			18 ± 1	19 ± 1	1.3×10^7	1.7×10^7
TMS-Tet	0.8 ± 0.3	1.3 ± 0.3			200 ± 60	150 ± 30	8.3×10^8	1.9×10^8
F-Tet			2.0 ± 0.1	2.0 ± 0.1	160 ± 10	210 ± 10	1.9×10^7	8.8×10^7

Figure 7. Data for Me-Tet, TMS-Tet, and F-Tet. (a) Ground-state FT-IR absorption in the 2200 cm^{-1} region. (b) Time-evolution of the CN stretch in F-Tet film on CaF2. The substrate response and coherence artifacts give rise to the offsets between the spectra at the early times. (c) Species associated singlet and triplet IR spectra corresponding to the global fit to the kinetic model.

formed triplets are trapped. The error bars on the triplet yields measured in these systems are too large to permit a quantitative estimate of the triplet trapping efficiency (see below).

We applied global kinetic analysis to the fsTA data obtained for each film using a sequential decay model. Details of the modeling are given in the SI, Section S5, and the kinetic parameters are shown in Table 2. It is worth noting that the rates will actually be distributed to some degree in the real system owing to the intrinsic heterogeneity of the film; by using a single value, we are assuming that the distribution of rates in the system is narrow. The good agreement with the relatively simple kinetic model and the reasonable uncertainties of the values extracted from the fits support our assumptions for this system.

The results of the global analysis of the Me-Tet and TMS-Tet films (Figures S15 and S16) show a similar ~1−2 ps relaxation for each film, where the spectra of the initial and relaxed excited states are highly similar. The inclusion of singlet−singlet annihilation in the high-fluence data yields rates that are in good agreement with the low-fluence data, suggesting that early dynamics are well accounted for. Singlet fission proceeds from the relaxed state in each film. In Me-Tet, SF is highly efficient and occurs with an 18 ps time constant, while SF in TMS-Tet is significantly slower, producing the

triplet population in around 200 ps. The kinetic models applied to the data are simplified in the sense that alternative decay pathways back to the ground state are neglected, as they are presumed to be out-competed by the faster SF process. This approximation is reasonable given the ~10 ns S_1 lifetime of the monomeric tetracene chromophores in solution and the agreement between the model populations from the fits and the independently calculated triplet yields discussed below.

Unlike in the other derivatives, the fsTA data for the F-Tet films indicate that the singlet population relaxes through an intermediate electronic state that mediates the singlet fission process (Figure 6). The spectra show the formation in 2 ps of new absorption bands at 895 and 1010 nm concomitant with an apparent redshift of the band at 540 nm and the loss of the S_1 feature at 1200 nm. The rate of this initial decay is similar to the relaxation times observed in other derivatives. However, since the relaxation process is along the same S_1 electronic state surface, there is minimal population loss preceding the formation of the intermediate state. Following the decay of such an intermediate, SF occurs in $\tau = 210$ ps to give the triplet of F-Tet indicated by the growth of the absorption feature at 560 nm.

The spectral evolution and kinetics for F-Tet on glass were similarly observed for the F-Tet thin film on a sapphire disk

(Figures S20 and S21). Given the higher thermal conductivity of the latter substrate,[48,49] as well as the similar kinetics indicated by both high- and low-fluence fsTA spectroscopy, thermal effects on SF in these films caused by laser irradiation are negligible.

The films were also studied with femtosecond transient infrared (fsIR) spectroscopy, where the cyano group provides a vibrational tag that allows us to probe the singlet-fission dynamics in the IR region around 2200 cm^{-1}. The ground-state cyano stretch was observed at 2199, 2201, and 2204 cm^{-1} for the Me-Tet, TMS-Tet, and F-Tet thin films, respectively, following the trend according to the electron-donating power of the substituents (Figure 7). Representative fsIR spectra are also given in Figure 7, in addition to the results of a global spectral analysis. This analysis permitted the extraction of the species-associated spectra for the singlet excited and triplet states for each derivative; further details are given in the SI. Upon photoexcitation at the 0−0 band (550−570 nm, 2 μJ/ pulse), in addition to the GSB peaks, an ESA band at lower frequency was observed at early times at 2181 (Me-Tet) and 2196 cm^{-1} (F-Tet), although the low optical density of the TMS-Tet film prevented a peak assignment at early times. These features subsequently shift to slightly higher frequencies at 2183 (Me-Tet), 2194 (TMS-Tet), and 2198 cm^{-1} (F-Tet). The extent of peak separation between the GSB and ESA follows, once again, the electron-donating power of the substituents, suggesting charge-transfer character in the excited states. The ESA signal shows biexponential decays with time constants similar to those observed by fsTA. As the remaining signal persists for much longer than 8 ns, we conclude that this shift corresponds to the formation of the triplet state by SF. These data suggest that the singlet and triplet states are structurally similar, leading to only a small shift between the S_1 and T_1 spectra. However, for F-Tet the T_1 species-associated spectrum shows a sharpening of the ESA band compared to its precursor spectrum; from fitting the spectra to the sum of two Lorentzians (SI, Section S6), the full width at half-maximum (fwhm) is reduced by 10−20%. The much lower signal-to-noise ratio in the fsIR spectra for Me-Tet and TMS-Tet prohibits making an adequate comparison of the fwhm, but such a peak sharpening may indicate that the triplet state is more localized.

Triplet Yield Calculations. Nanosecond transient absorp-tion (nsTA) spectroscopy was used to measure the triplet signal and to calculate triplet quantum yields. Other methods of triplet yield determination necessitate spectrally independent T_1 ESA signals to kinetically or quantitatively track the triplet population.[19,50] Because of complicated overlap of the S_1 and T_1 ESA with the GSB signals and spectral variations across the series of molecules, the singlet depletion method was chosen for triplet yield analysis. This method, which has been outlined by Carmichael and Hug,[51] has been previously applied to calculate triplet yields in SF systems.[21,22,26,37]

For this analysis, we use a nsTA trace at a 50 ns delay, where only the triplet population is present, and quantitate the amount of GSB signal in the transient trace. By comparing this value to the predicted bleach, based on the excitation density and film absorption spectrum, we can determine the triplet quantum yield. The detailed procedure of this analysis is included in the SI. The results indicate that efficient SF occurs in both the Me-Tet ($\varphi_T = 195 \pm 30\%$) and F-Tet ($\varphi_T = 210 \pm 42\%$) derivatives. Both of these values are consistent with the high yield of triplet observed in the fsTA data, and support the assumption that other decay processes are negligible from either the singlet or intermediate states and suggest that the model populations are reasonable surrogates for the triplet yields in this case. For TMS-Tet, we observe marginal triplet yields ($\varphi_T = 60 \pm 25\%$), again consistent with the transient absorption data. This implies that the unfavorable interchro-mophore distances determined by the steric bulk of the TMS group has a dramatic effect on the SF efficiency in the crystalline films.

◼ DISCUSSION

Singlet Fission Efficiency and π Contact. The geometry of the SF-active dimer pair in H-Tet was previously unresolved due to the presence of two closely interacting dimer pair interactions in the crystal structure (Figure 1). Close similarities between the H-Tet α interaction and the dimer pair in the Me-Tet crystal structure allow for comparison of the SF kinetics and thus the structural origin of the SF dynamics in this series of molecules.

Given the highly efficient SF observed in both H- and Me-Tet films, the α interaction (short axis slip) can provide sufficiently good coupling for SF. However, since the slippage and π−π distance for the α interaction is larger in H-Tet than those in Me-Tet (Table 1), yet faster overall SF (~13 ps)[40] is observed for H-Tet, SF is likely more effectively driven by the closely π-stacked (3.31 Å), but less well overlapping β dimer pair (long axis slip). This finding also suggests that a large degree of π contact or small lateral displacement is not necessary for rapid and efficient SF in the solid state.

The observation of slower SF in TMS-Tet points to the importance of the π−π distance in enabling the coupling necessary for SF. The large steric bulk of the TMS group results in a very long π−π distance of 4.17 Å. Because of this long distance between neighboring chromophores, SF is highly inefficient in the annealed TMS-Tet film ($\varphi_T \approx 60\%$; nearly 0% in unannealed film, data not shown). Kinetic analysis of the SF dynamics in TMS-Tet also point to much poorer SF in this derivative than in the other Tet derivatives. In the case of the annealed film, an apparent $\tau_{SF} = 200$ ps is observed. Given that the geometry of the dimer pair in TMS-Tet is nearly identical to the Me-Tet dimer pair except for the π−π distance (Me-Tet: 3.94 Å, TMS-Tet: 4.17 Å), we assign the differences in SF between the two compounds to the difference in their π contact. The role of the interchromophore distance in tuning the strength of the SF coupling interaction has been previously explored in pentacene.[52] Our results indicate that the increase in π−π distance from 3.94 to 4.17 Å is significant enough to reduce dramatically the SF efficiency in these Tet derivatives.

Singlet Fission Intermediate. The fsTA data indicate that the SF process in F-Tet involves the participation of an intermediate prior to triplet formation. Depopulation of the $^1(S_1S_0)$ state, as evidenced by the decay of the NIR absorption band at ~1200 nm, is associated with the growth of bands at 890 and 1010 nm (Figure 6). These bands correlate well with the absorption bands for the tetracene anion radical and radical cation, which occur in low temperature glasses at about 820 and 880 nm, respectively.[53,54] The longer wavelengths observed for F-Tet may be a result of the additional substituents conjugated to the tetracenes used in this study. Indeed, NIR absorptions at ~870 and 980 nm were observed for the cation and anion of F-Tet, generated electrochemically in solution (see Figures S26−28 in the SI, Section 8). Furthermore, the decay of these features is concomitant with the growth of T_1 absorption at 560 nm, which suggests the role of an intermediate in the SF

mechanism of F-Tet. The close resemblance of these features, particularly the NIR bands, to the tetracene radical ions suggests the intermediate state we are observing has significant charge transfer (CT) character. Due to their ability to couple the initial $^1(S_1S_0)$ state to the $^1(T_1T_1)$ triplet pair state, CT states have been implicated as either real or virtual intermediates in the SF process.[48,55] A slightly modified kinetic scheme considering the participation of the putative $^1(T_1T_1)$ state is also given in the SI, Section S5.

The observation of a CT intermediate in the SF mechanism for F-Tet indicates that CT state formation may be mechanistically important for SF in tetracene-based materials. The fluorine substituents on F-Tet may position its CT state energy close enough to that of $^1(S_1S_0)$ to make it an accessible real intermediate preceding $^1(T_1T_1)$ formation, while not stabilizing the CT state so much that it becomes a trap state. We find that the CT state forms in τ ~ 2 ps, and decays to the $^1(T_1T_1)$ state in τ ~ 200 ps. The relatively slow CT → $^1(T_1T_1)$ rate in F-Tet may be a result of a small free energy change for the CT → $^1(T_1T_1)$ process.[56] The high SF yield can be attributed to the competition of this rate with a comparatively slow charge recombination to ground state that results from the large free energy change for this process, which should be within the Marcus inverted region. Thus, CT state recombination to ground state can be safely neglected in the kinetic model, and the resultant triplet population agrees well with the yield obtained from the nsTA measurements.

CONCLUSIONS

By comparing the SF rate in H-Tet and Me-Tet, we find that the long-axis slipped β dimer pair likely contributes to the more rapid SF in H-Tet, while short-axis slipped α dimer geometry also provides good coupling for SF. Our results also indicate that there exists a threshold for efficient SF in the π-stacking interaction between neighboring chromophores in the solid state. Substantially increasing this distance to 4.17 Å in TMS-Tet results in slow (~200 ps) and inefficient (φ_T ≈ 60%) SF. Photoexcitation of the F-Tet derivative populates an intermediate CT state that precedes $^1(T_1T_1)$ formation. We find that population of this CT state does not preclude efficient SF (φ_T ≈ 200%). Rather, the kinetic evidence suggests that this state enables the formation of the multiexciton state in a CT-mediated SF mechanism. These substituent effects highlight the importance of coupling and reveal the role of CT state intermediates in the SF mechanism for tetracene derivatives.

ASSOCIATED CONTENT

* Supporting Information

Experimental details and characterization for new compounds as well as copies of ^1H, ^{13}C, and ^{19}F NMR spectra, full data set for the high fluence femtosecond-transient absorption, kinetic modeling, femtosecond-infrared spectroscopy analysis, film nanosecond-transient absorption, spectroelectrochemistry, triplet yield calcu-lations, and DFT calculations (PDF). X-ray crystallographic data for F-TET (CIF).
X-ray crystallographic data for TMS-Tet (CIF). X-ray crystallographic data for intermediate cumulene S4a (CIF).

X-ray crystallographic data for intermediate cumulene S4b (CIF).

AUTHOR INFORMATION

Corresponding Authors
*E-mail: m-wasielewski@northwestern.edu.
*E-mail: diederich@org.chem.ethz.ch.
*E-mail: yi-lin.wu@northwestern.edu.
ORCID
Catherine M. Mauck: 0000-0002-6432-9724
Ryan M. Young: 0000-0002-5108-0261
Yi-Lin Wu: 0000-0003-0253-1625
Francois Diederich: 0000-0003-1947-6327
Michael R. Wasielewski: 0000-0003-2920-5440
Notes
The authors declare no competing financial interest.

REFERENCES

(1) Congreve, D. N.; Lee, J.; Thompson, N. J.; Hontz, E.; Yost, S. R.; Reusswig, P. D.; Bahlke, M. E.; Reineke, S.; Van Voorhis, T.; Baldo, M. A. External Quantum Efficiency above 100% in a Singlet-Exciton-Fission-Based Organic Photovoltaic Cell. Science 2013, 340, 334−337.
(2) Hanna, M. C.; Nozik, A. J. Solar Conversion Efficiency of Photovoltaic and Photoelectrolysis Cells with Carrier Multiplication Absorbers. J. Appl. Phys. 2006, 100, 074510/1−074510/8.
(3) Shockley, W.; Queisser, H. J. Detailed Balance Limit of Efficiency of P-N Junction Solar Cells. J. Appl. Phys. 1961, 32, 510−519.
(4) Berkelbach, T. C.; Hybertsen, M. S.; Reichman, D. R. Microscopic Theory of Singlet Exciton Fission. II. Application to Pentacene Dimers and the Role of Superexchange. J. Chem. Phys. 2013, 138, 114103.
(5) Zheng, J.; Xie, Y.; Jiang, S.; Lan, Z. Ultrafast Nonadiabatic Dynamics of Singlet Fission: Quantum Dynamics with the Multilayer Multiconfigurational Time-Dependent Hartree (ML-MCTDH) Meth-od. J. Phys. Chem. C 2016, 120, 1375−1389.
(6) Fuemmeler, E. G.; et al. A Direct Mechanism of Ultrafast Intramolecular Singlet Fission in Pentacene Dimers. ACS Cent. Sci. 2016, 2, 316−324.
(7) Smith, M. B.; Michl, J. Singlet Fission. Chem. Rev. 2010, 110, 6891−6936.
(8) Burdett, J. J.; Bardeen, C. J. Quantum Beats in Crystalline Tetracene Delayed Fluorescence Due to Triplet Pair Coherences Produced by Direct Singlet Fission. J. Am. Chem. Soc. 2012, 134, 8597−8607.

(9) Chan, W.-L.; Ligges, M.; Jailaubekov, A.; Kaake, L.; Miaja-Avila, L.; Zhu, X.-Y. Observing the Multiexciton State in Singlet Fission and Ensuing Ultrafast Multielectron Transfer. Science 2011, 334, 1541−1545.

(10) Greyson, E. C.; Vura-Weis, J.; Michl, J.; Ratner, M. A. Maximizing Singlet Fission in Organic Dimers: Theoretical Investigation of Triplet Yield in the Regime of Localized Excitation and Fast Coherent Electron Transfer. J. Phys. Chem. B 2010, 114, 14168−14177.

(11) Zimmerman, P. M.; Bell, F.; Casanova, D.; Head-Gordon, M. Mechanism for Singlet Fission in Pentacene and Tetracene: From Single Exciton to Two Triplets. J. Am. Chem. Soc. 2011, 133, 19944−19952.

(12) Bixon, M.; Jortner, J. Electron Transfer via Bridges. J. Chem. Phys. 1997, 107, 5154−5170.

(13) Goldsmith, R. H.; Wasielewski, M. R.; Ratner, M. A. Electron Transfer in Multiply Bridged Donor-Acceptor Molecules: Dephasing and Quantum Coherence. J. Phys. Chem. B 2006, 110, 20258−20262.

(14) Makri, N.; Sim, E.; Makarov, D. E.; Topaler, M. Long-Time Quantum Simulation of the Primary Charge Separation in Bacterial Photosynthesis. Proc. Natl. Acad. Sci. U. S. A. 1996, 93, 3926−3931.

(15) Singh, S.; Jones, W. J.; Siebrand, W.; Stoicheff, B. P.; Schneider, W. G. Laser Generation of Excitons and Fluorescence in Anthracene Crystals. J. Chem. Phys. 1965, 42, 330−342.

(16) Swenberg, C. E.; Stacy, W. T. Bimolecular Radiationless Transitions in Crystalline Tetracene. Chem. Phys. Lett. 1968, 2, 327− 328.

(17) Geacintov, N.; Pope, M.; Vogel, F. Effect of Magnetic Field on the Fluorescence of Tetracene Crystals: Exciton Fission. Phys. Rev. Lett. 1969, 22, 593−596.

(18) Musser, A. J.; Maiuri, M.; Brida, D.; Cerullo, G.; Friend, R. H.; Clark, J. The Nature of Singlet Exciton Fission in Carotenoid Aggregates. J. Am. Chem. Soc. 2015, 137, 5130−5139.

(19) Wang, C.; Tauber, M. J. High-Yield Singlet Fission in a Zeaxanthin Aggregate Observed by Picosecond Resonance Raman Spectroscopy. J. Am. Chem. Soc. 2010, 132, 13988−13991.

(20) Dillon, R. J.; Piland, G. B.; Bardeen, C. J. Different Rates of Singlet Fission in Monoclinic Versus Orthorhombic Crystal Forms of Diphenylhexatriene. J. Am. Chem. Soc. 2013, 135, 17278−17281.

(21) Eaton, S. W.; Miller, S. A.; Margulies, E. A.; Shoer, L. E.; Schaller, R. D.; Wasielewski, M. R. Singlet Exciton Fission in Thin Films of tert-Butyl-Substituted Terrylenes. J. Phys. Chem. A 2015, 119, 4151−4161.

(22) Eaton, S. W.; et al. Singlet Exciton Fission in Polycrystalline Thin Films of a Slip-Stacked Perylenediimide. J. Am. Chem. Soc. 2013, 135, 14701−14712.

(23) Ma, L.; Tan, K. J.; Jiang, H.; Kloc, C.; Michel-Beyerle, M.-E.; Gurzadyan, G. G. Excited-State Dynamics in an α-Perylene Single Crystal: Two-Photon- and Consecutive Two-Quantum-Induced Singlet Fission. J. Phys. Chem. A 2014, 118, 838−843.

(24) Musser, A. J.; Al-Hashimi, M.; Maiuri, M.; Brida, D.; Heeney, M.; Cerullo, G.; Friend, R. H.; Clark, J. Activated Singlet Exciton Fission in a Semiconducting Polymer. J. Am. Chem. Soc. 2013, 135, 12747−12754.

(25) Busby, E.; Xia, J.; Wu, Q.; Low, J. Z.; Song, R.; Miller, J. R.; Zhu, X.-Y.; Campos, Luis M.; Sfeir, M. Y. A Design Strategy for Intramolecular Singlet Fission Mediated by Charge-Transfer States in Donor−Acceptor Organic Materials. Nat. Mater. 2015, 14, 426− 433.

(26) Hartnett, P. E.; Margulies, E. A.; Mauck, C. M.; Miller, S. A.; Wu, Y.; Wu, Y.-L.; Marks, T. J.; Wasielewski, M. R. Effects of Crystal Morphology on Singlet Exciton Fission in Diketopyrrolopyrrole Thin Films. J. Phys. Chem. B 2016, 120, 1357−1366.

(27) Johnson, J. C.; Nozik, A. J.; Michl, J. High Triplet Yield from Singlet Fission in a Thin Film of 1,3-Diphenylisobenzofuran. J. Am. Chem. Soc. 2010, 132, 16302−16303.

(28) Ryerson, J. L.; Schrauben, J. N.; Ferguson, A. J.; Sahoo, S. C.; Naumov, P.; Havlas, Z.; Michl, J.; Nozik, A. J.; Johnson, J. C. Two

Thin Film Polymorphs of the Singlet Fission Compound 1,3-Diphenylisobenzofuran. J. Phys. Chem. C 2014, 118, 12121−12132.

(29) Burdett, J. J.; Gosztola, D.; Bardeen, C. J. The Dependence of Singlet Exciton Relaxation on Excitation Density and Temperature in Polycrystalline Tetracene Thin Films: Kinetic Evidence for a Dark Intermediate State and Implications for Singlet Fission. J. Chem. Phys. 2011, 135, 214508.

(30) Chan, W.-L.; Ligges, M.; Zhu, X.-Y. The Energy Barrier in Singlet Fission Can Be Overcome through Coherent Coupling and Entropic Gain. Nat. Chem. 2012, 4, 840−845.

(31) Grumstrup, E. M.; Johnson, J. C.; Damrauer, N. H. Enhanced Triplet Formation in Polycrystalline Tetracene Films by Femtosecond Optical-Pulse Shaping. Phys. Rev. Lett. 2010, 105, 257403/1−257403/ 4.

(32) Korovina, N. V.; Das, S.; Nett, Z.; Feng, X.; Joy, J.; Haiges, R.; Krylov, A. I.; Bradforth, S. E.; Thompson, M. E. Singlet Fission in a Covalently Linked Cofacial Alkynyltetracene Dimer. J. Am. Chem. Soc. 2016, 138, 617−627.

(33) Lukman, S.; et al. Tuneable Singlet Exciton Fission and Triplet-Triplet Annihilation in an Orthogonal Pentacene Dimer. Adv. Funct. Mater. 2015, 25, 5452−5461.

(34) Ma, L.; Zhang, K.; Kloc, C.; Sun, H.; Michel-Beyerle, M. E.; Gurzadyan, G. G. Singlet Fission in Rubrene Single Crystal: Direct Observation by Femtosecond Pump-Probe Spectroscopy. Phys. Chem. Chem. Phys. 2012, 14, 8307−8312.

(35) Müller, A. M.; Avlasevich, Y. S.; Schoeller, W. W.; Müllen, K.; Bardeen, C. J. Exciton Fission and Fusion in Bis(tetracene) Molecules with Different Covalent Linker Structures. J. Am. Chem. Soc. 2007, 129, 14240−14250.

(36) Roberts, S. T.; McAnally, R. E.; Mastron, J. N.; Webber, D. H.; Whited, M. T.; Brutchey, R. L.; Thompson, M. E.; Bradforth, S. E. Efficient Singlet Fission Discovered in a Disordered Acene Film. J. Am. Chem. Soc. 2012, 134, 6388−6400.

(37) Sanders, S. N.; et al. Quantitative Intramolecular Singlet Fission in Bipentacenes. J. Am. Chem. Soc. 2015, 137, 8965−8972.

(38) Walker, B. J.; Musser, A. J.; Beljonne, D.; Friend, R. H. Singlet Exciton Fission in Solution. Nat. Chem. 2013, 5, 1019−1024.

(39) Zirzlmeier, J.; Lehnherr, D.; Coto, P. B.; Chernick, E. T.; Casillas, R.; Basel, B. S.; Thoss, M.; Tykwinski, R. R.; Guldi, D. M. Singlet Fission in Pentacene Dimers. Proc. Natl. Acad. Sci. U. S. A. 2015, 112, 5325−5330.

(40) Margulies, E. A.; Wu, Y.-L.; Gawel, P.; Miller, S. A.; Shoer, L. E.; Schaller, R. D.; Diederich, F.; Wasielewski, M. R. Sub-Picosecond Singlet Exciton Fission in Cyano-Substituted Diaryltetracenes. Angew. Chem., Int. Ed. 2015, 54, 8679−8683.

(41) Gawel, P.; Dengiz, C.; Finke, A. D.; Trapp, N.; Boudon, C.; Gisselbrecht, J.-P.; Diederich, F. Synthesis of Cyano-Substituted Diaryltetracenes from Tetraaryl[3]Cumulenes. Angew. Chem., Int. Ed. 2014, 53, 4341−4345.

(42) Young, R. M.; Dyar, S. M.; Barnes, J. C.; Juríček, M.; Stoddart, J. F.; Co, D. T.; Wasielewski, M. R. Ultrafast Conformational Dynamics of Electron Transfer in Exbox4+⊂Perylene. J. Phys. Chem. A 2013, 117, 12438−12448.

(43) Hartnett, P. E.; Mauck, C. M.; Harris, M. A.; Young, R. M.; Wu, Y.-L.; Marks, T. J.; Wasielewski, M. R. Influence of Anion Delocalization on Electron Transfer in a Covalent Porphyrin Donor-Perylenediimide Dimer Acceptor System. J. Am. Chem. Soc. 2017, 139, 749−756.

(44) Campbell, R. B.; Robertson, J. M.; Trotter, J. The Crystal Structure of Hexacene, and a Revision of the Crystallographic Data for Tetracene. Acta Crystallogr. 1962, 15, 289−290.

(45) Anthony, J. E.; Eaton, D. L.; Parkin, S. R. A Road Map to Stable, Soluble, Easily Crystallized Pentacene Derivatives. Org. Lett. 2002, 4, 15−18.

(46) Lim, S.-H.; Bjorklund, T. G.; Spano, F. C.; Bardeen, C. J. Exciton Delocalization and Superradiance in Tetracene Thin Films and Nanoaggregates. Phys. Rev. Lett. 2004, 92, 107402.

(47) Kasha, M.; Rawls, H. R.; Ashraf El-Bayoumi, M. The Exciton Model in Molecular Spectroscopy. Pure Appl. Chem. 1965, 11, 371− 392.

(48) Margulies, E. A.; Logsdon, J. L.; Miller, C. E.; Ma, L.; Simonoff, E.; Young, R. M.; Schatz, G. C.; Wasielewski, M. R. Direct Observation of a Charge Transfer State Preceding High Yield Singlet Fission in Terrylenediimide Thin Films. J. Am. Chem. Soc. 2017, 139, 663−671.

(49) Rao, A.; Wilson, M. W. B.; Albert-Seifried, S.; Di Pietro, R.; Friend, R. H. Photophysics of Pentacene Thin Films: The Role of Exciton Fission and Heating Effects. Phys. Rev. B: Condens. Matter Mater. Phys. 2011, 84, 195411/1−195411/8.

(50) Burdett, J. J.; Müller, A. M.; Gosztola, D.; Bardeen, C. J. Excited State Dynamics in Solid and Monomeric Tetracene: The Roles of Superradiance and Exciton Fission. J. Chem. Phys. 2010, 133, 144506.

(51) Carmichael, I.; Hug, G. L. Triplet−Triplet Absorption Spectra of Organic Molecules in Condensed Phases. J. Phys. Chem. Ref. Data 1986, 15, 1−250.

(52) Zeng, T.; Hoffmann, R.; Ananth, N. The Low-Lying Electronic States of Pentacene and Their Roles in Singlet Fission. J. Am. Chem. Soc. 2014, 136, 5755−5764.

(53) Shida, T.; Iwata, S. Electronic Spectra of Ion Radicals and Their Molecular Orbital Interpretation. Iii. Aromatic Hydrocarbons. J. Am. Chem. Soc. 1973, 95, 3473−3483.

(54) Szczepanski, J.; Drawdy, J.; Wehlburg, C.; Vala, M. Vibrational and Electronic Spectra of Matrix-Isolated Tetracene Cations. Chem. Phys. Lett. 1995, 245, 539−548.

(55) Johnson, J. C.; et al. Toward Designed Singlet Fission: Solution Photophysics of Two Indirectly Coupled Covalent Dimers of 1,3-Diphenylisobenzofuran. J. Phys. Chem. B 2013, 117, 4680−4695.

(56) Teichen, P. E.; Eaves, J. D. A Microscopic Model of Singlet Fission. J. Phys. Chem. B 2012, 116, 11473−11481.